

Permeability of Wilcox shale and its effective pressure law

Ohmyoung Kwon, Andreas K. Kronenberg, Anthony F. Gangi,
and Brann Johnson

Center for Tectonophysics, Department of Geology and Geophysics
Texas A&M University, College Station, Texas, USA

Abstract. The permeability of illite-rich shale from the Wilcox formation has been measured as a function of effective pressure for bedding-parallel flow of 1 M NaCl pore fluid. Permeability k decreases from $\sim 300 \times 10^{-21} \text{ m}^2$ to $3 \times 10^{-21} \text{ m}^2$ as effective pressure P_e is increased from 3 to 12 MPa; these values confirm that shales form effective barriers to fluid transport in sedimentary strata over extended geologic times. The variation of k with P_e for Wilcox shale is given by $k = k_0 [1 - (P_e/P_1)^m]^3$, where $P_1 = 19.3 (\pm 1.6)$ MPa and $m = 0.159 (\pm 0.007)$. The value of k_0 for Wilcox shale is of the order of 10^{-17} m^2 and may vary among samples by as much as 70%. Effective pressure is given in terms of the external confining pressure P_c and internal pore pressure P_p by $P_e = P_c - \chi P_p$, where $\chi = 0.99 (\pm 0.06)$. While our measurements yield $\chi = \sim 1$ for shale with a clay content of $\sim 45\%$, others have reported χ values for clay-bearing sandstones that rise from ~ 0.75 to 7.1 with increasing clay content (from 0 to 20%). The trends between χ and clay content revealed by these comparisons imply that the value of χ depends upon the relative distributions of compliant clay minerals and other stiffer minerals. These values of χ also suggest that effective pressures within interbedded sandstones and shales may differ, even at the same equilibrium P_c and P_p conditions.

1. Introduction

Fluid transport properties of sandstones are strongly influenced by the occurrence of clay minerals [Stalder, 1973; Nagtegaal, 1979; Pallatt *et al.*, 1984; Ives, 1987; Howard, 1992], and permeabilities of shales and other argillaceous rocks are many orders of magnitude smaller than those of clastic rocks with low clay contents [Young *et al.*, 1964; Lin, 1978; Magara, 1978; Neglia, 1979; Brace, 1980; Bredehoeft *et al.*, 1983; Katsube *et al.*, 1991; Neuzil, 1994; Schlomer and Krooss, 1997; Dewhurst *et al.*, 1998, 1999]. As a result, subsurface fluid flow may be very rapid within sandstones, allowing equilibrium pore pressures to be established in relatively short time intervals, while flow through shales may be so slow that departures in pore pressure from the hydrostat are supported over geologically significant time intervals [Dickinson, 1953; Bredehoeft and Hanshaw, 1968; Dickey *et al.*, 1968; Magara, 1971; Chapman, 1972, 1994a, 1994b; Bruce, 1973, 1984; Schmidt, 1973; Bishop, 1979; Plumley, 1980; Berg and Habeck, 1982; Harrison and Summa, 1991; Caillet, 1993; Bigelow, 1994; Deming, 1994]. With burial, reductions in porosity of clay-bearing sediments are as great as, or exceed, those noted for more sandy intervals [Bryant *et al.*, 1975; Addis and Jones, 1985; Dzevanishir *et al.*, 1986; Bennett *et al.*, 1989; Kim *et al.*, 1999], leading to increases in pore pressure or the expulsion of fluid. With increasing burial and compaction, further reductions in permeability are expected [e.g., Young *et al.*, 1964; Neglia, 1979; Brace, 1980; Morrow *et al.*, 1984; Dewhurst *et al.*, 1998].

Laboratory measurements of permeabilities reported for intact shales, mudstones, and clay aggregates subjected to hydrostatic pressures and unidirectional loads vary from 10^{-16} m^2 to 10^{-23} m^2 , and numerous studies have shown that permeabili-

ties decrease with externally applied stress [e.g., Young *et al.*, 1964; Lin, 1978; Magara, 1978; Bredehoeft *et al.*, 1983; Morrow *et al.*, 1984; Katsube *et al.*, 1991; Vasseur *et al.*, 1995; Dewhurst *et al.*, 1999] and decreased porosity [Bryant *et al.*, 1975; Silva *et al.*, 1981; Tavenas *et al.*, 1983; Bennett *et al.*, 1989; Schlomer and Krooss, 1997; Dewhurst *et al.*, 1998]. A variety of nonlinear relations have been proposed between permeability, porosity, and pressure applied to shales and mudstones, including exponential and power laws between permeability and porosity [Silva *et al.*, 1981; Tavenas *et al.*, 1983; Bennett *et al.*, 1989; Schlomer and Krooss, 1997; Dewhurst *et al.*, 1998] and similar laws between permeability and pressure [Lin, 1978; Katsube *et al.*, 1991; Vasseur *et al.*, 1995; Dewhurst *et al.*, 1999]. However, most of these relations have been chosen on an empirical basis to fit experimental data. Correlations between permeability and porosity are problematic due to unconnected porosity that does not contribute to fluid flow and potential variations in tortuosity that lead to significant scatter in permeability-porosity data [e.g., Stalder, 1973; Katsube *et al.*, 1991; Howard, 1992; Schlomer and Krooss, 1997]. Moreover, measurements of shale permeabilities at known values of effective pressure have been limited owing to (1) uncertainties in true internal pore pressure and (2) the long experimental times required to measure transport properties at low flow rates and to raise effective pressure at rates that allow pore pressures to equilibrate within specimens prior to measuring permeability. In all previous determinations of shale permeability that we are aware of, effective pressure P_e has been assumed, without demonstration, to be the simple difference between confining pressure P_c and pore fluid pressure P_p .

While the earliest laws of effective pressure P_e for soil and rock properties [e.g., Terzaghi, 1923, 1925, 1936] define P_e as the difference between confining and pore pressures ($P_c - P_p$), transport properties for a variety of rock types exhibit less sensitivity to pore pressure than to confining pressure with P_e

Copyright 2001 by the American Geophysical Union.

Paper number 2001JB000273.
0148-0227/01/2001JB000273\$09.00

given by $(P_c - \chi P_p)$ and values of χ of 0.6–0.75 for quartzose sandstones [David and Darot, 1989] and 0.5–1.0 for granites and crystalline rocks [Kranz et al., 1979; Bernabe, 1986, 1987; Morrow et al., 1986]. The effective pressure law coefficient χ may differ for different material properties of the same rock, but χ generally takes on values (≤ 1) consistent with models of porous media with fluid-filled pores and homogeneous elastic properties of the solid [Nur and Byerlee, 1971; Robin, 1973; Garg and Nur, 1973; Paterson, 1978; Kranz et al., 1979; Walsh, 1981; Berryman, 1992]. Although χ is generally taken to be constant, yielding a linear expression for effective pressure, χ may itself be a function of pressures P_c or P_p , or microstructural changes in pore structure [Fatt, 1958, 1959; Nur and Byerlee, 1971; Todd and Simmons, 1972; Christensen and Wang, 1985; Bernabe, 1986, 1987; Gangi and Carlson, 1996].

Pore geometries and transport properties of sandstones are altered markedly by clay minerals [e.g., Bernabe, 1991], and values of χ for fluid transport in clay-bearing sandstones are anomalously large. Effective pressure law coefficients χ for permeabilities of clay-bearing sandstones vary from ~ 1.0 to 7.1, corresponding to clay contents of ~ 0 to 20%, respectively [Zoback, 1975; Zoback and Byerlee, 1975, 1976; Walls and Nur, 1979]. Values of $\chi > 1$ require explanation, and Zoback and Byerlee [1975] offer a conceptual model to explain high sensitivities to pore pressure based on highly compliant clays lining the pores of sandstones. Berryman [1992, 1993] developed this model further as a special case of the elastic response of heterogeneous porous media and found that large χ values depend on the distributions of clays relative to pore space and quantitative values of pore compressibility. These models have yet to be tested for clay-bearing sandstones, and just how they extend to the clay contents characteristic of shales ($\sim 50\%$) is unclear.

In this paper, we present the results of an experimental study of permeability of a low-porosity, illite-rich shale from the Wilcox formation designed to determine its effective pressure law for pore fluid flow and the relationship between permeability and effective pressure. Our results show that χ very nearly equals unity, in support of assumptions made in previous studies of shale permeability, and they suggest a significant change in the trend exhibited by clay-bearing sandstones between the value of χ and clay content as clay content exceeds $\sim 20\%$.

2. Background

Physical properties of porous rocks in the presence of fluid commonly depend on both confining pressure and pore pressure according to an effective pressure law. The effective pressure P_e of a rock is defined such that a physical property Q determined at some confining pressure P_c and pore pressure P_p has the same value as that observed at a confining pressure equal to the effective pressure when the pore pressure is zero [Robin, 1973]. Thus, given that Q depends on P_c and P_p , the law of effective pressure for that property $P_e = f(P_c, P_p)$ [e.g., Walsh, 1981; Gangi and Carlson, 1996] reduces the number of independent variables needed to specify Q according to

$$Q(P_e) = Q\{f(P_c, P_p)\}. \quad (1)$$

As the relationship $f(P_c, P_p)$ depends upon the material property under consideration, the value of P_e may differ for different properties at a given set of P_c, P_p values.

Porosities, connected-pore networks, and distributions of pore apertures are critical to the transport properties of rocks, and a number of expressions have been evaluated for the effective pressure of a porous, fluid-saturated solid undergoing elastic deformation [Biot, 1941; Biot and Willis, 1957; Skempton, 1961; Nur and Byerlee, 1971; Robin, 1973; Garg and Nur, 1973; Berryman, 1992]. Effective pressures governing volumetric strain of porous rocks can be specified in macroscopic terms as

$$P_e = P_c - (1 - \kappa/\kappa_s)P_p, \quad (2)$$

where κ is the bulk modulus of the rock without a pore fluid and κ_s is the intrinsic bulk modulus of the solid, absent any pores [Skempton, 1961; Nur and Byerlee, 1971; Berryman, 1992]. However, if pore volume of the same solid is considered, the governing effective pressure law is expressed as

$$P_e = P_c - [1 - \phi\kappa/(\kappa_s - \kappa)]P_p, \quad (3)$$

where ϕ is porosity and the moduli κ and κ_s are defined as in (2) [Robin, 1973]. Assuming that fluid flow occurs through rough channel-like pores and cracks [Gangi, 1978; Walsh, 1981], effective pressure for permeability may be expressed at the scale of asperities. Equating P_e with an asperity pressure P_a across a loaded crack or grain contact,

$$P_e = P_a = P_c - (1 - A_c/A)P_p, \quad (4)$$

where A is the total surface area of the cracks (or pores) and A_c is the true area of loaded contacts [Gangi and Carlson, 1996].

Many other expressions for effective pressure have been derived, but experimentally determined effective pressures have generally been expressed simply as

$$P_e = P_c - \chi P_p, \quad (5)$$

where χ values determined for volumetric compaction, porosity, elasticity, and permeability are compatible with the corresponding terms of (2) to (4) and measured poroelastic response [e.g., Fatt, 1959; Skempton, 1961; Banthia et al., 1965; Nur and Byerlee, 1971; Todd and Simmons, 1972; Robin, 1973; Rice and Cleary, 1976; Gangi, 1978; Kranz et al., 1979; Walsh, 1981; Walsh and Brace, 1984; Carlson and Gangi, 1985; Christiansen and Wang, 1985; Gangi and Carlson, 1996]. Given that κ is nearly constant, equation (2) predicts a nearly constant value of $\chi \leq 1$. When κ is much smaller than κ_s , as noted for high-porosity rocks and soils (or A_c in (4) is much smaller than A), χ is predicted to be nearly equal to 1. Cemented quartz sandstones exhibit χ values for permeability of 0.6–1.2 [Walls and Nur, 1979; David and Darot, 1989], and pure quartz sands exhibit χ of almost exactly 1.0 [Zoback and Byerlee, 1976]. Drawing on the observed behavior of soils, values of χ for permeability of shales and clay aggregates have been assumed to equal 1 [Lin, 1978; Katsube et al., 1991; Vasseur et al., 1995; Dewhurst et al., 1998, 1999], yet this assumption does not follow from the observed sensitivity of permeability to pore pressure for cemented sandstones with clays [Zoback, 1975; Zoback and Byerlee, 1975; Walls and Nur, 1979].

Given that the effective pressure P_e is known, permeability can be determined as a function of just one macroscopic parameter $Q(P_e)$. At the pore scale, fluid flow depends upon the geometry, dimension, and connected nature of pores, with flow related to the fourth power of radius of tube-like conduits or the cube of the width of crack-like, planar conduits [e.g., Pater-

son, 1983; Walsh and Brace, 1984; Berryman and Blair, 1986, 1987; Thompson et al., 1987; Doyen, 1988; Bernabe, 1991; Fredrich et al., 1993; Blair et al., 1996]. Bulk permeabilities of rocks depend on flow through the entire network of connected pores of various geometries, as predicted by models based on equivalent channels or conduit networks of circular and elliptical cross sections [Gangi, 1976; Paterson, 1983; Seeburger and Nur, 1984; Walsh and Brace, 1984; Thompson et al., 1987; Doyen, 1988; Bernabe, 1991; David, 1993; David et al., 1990; Zhu et al., 1995, 1999]. While several criteria have been used to simulate pore shrinkage during compaction, changes in bulk permeability with effective pressure are most sensitive to changes in effective aperture of the more compliant crack-like pores.

Relationships between permeability and effective pressure have been evaluated for fractured rocks based upon asperity deformation models of rough cracks and the cubic relation between flow rate and aperture [Gangi, 1978; Walsh and Grosebaugh, 1979; Walsh, 1981; Walsh and Brace, 1984]. While the full populations of pores of varying geometries are not treated explicitly by these models, the variation in permeability with effective pressure has successfully matched experimental data for fractured as well as intact rocks [Jones, 1975; Nelson, 1976; Brace et al., 1968; Kranz et al., 1979; Jones and Owens, 1980; Witherspoon et al., 1980; Morrow et al., 1986; Brighenti, 1989] provided that a reference permeability can be specified at a reference pressure. For fluid flow through rough fractures with a power law (or fractal) size distribution of asperities, Gangi [1978] found permeability k to vary by a modified cubic function of P_e as

$$k = k_0[1 - (P_e/P_1)^m]^3, \quad (6)$$

where k_0 is the reference permeability at zero effective pressure, P_1 is an effective modulus of the asperities, and m is a constant (between 0 and 1). P_1 can be expressed as EA_r/A , where E is the Young's modulus and A_r/A is the fractional area of contact of the crack face at pressure [Gangi, 1978]. The value of constant m characterizes the distribution of asperity heights; m close to 1 represents a very smooth surface, while low values of m represent rough fracture surfaces. Using the same model of fluid flow through fractures with an exponential size distribution of asperities, Walsh [1981] found permeability to vary as

$$k = k_0[1 - (2^{1/2}h/a_0) \ln(P_e/P_0)]^3, \quad (7)$$

where k_0 is a reference permeability at effective pressure P_0 , h is the root-mean-square height distribution of asperities, and a_0 is the half width of the fracture aperture at the reference P_0 .

Differences in these relations are primarily due to differences in the assumed surface topographies of the cracks. From previous studies of shale (and mudstone) permeabilities, exponential and power laws between permeability and pressure (or unidirectional load) appear to fit experimental data equally well [Lin, 1978; Katsube et al., 1991; Vasseur et al., 1995; Dewhurst et al., 1999], and refinements in predicted k - P_e relationships of rocks would require analyses of asperity distributions and percolation models of the full populations of connected pores [e.g., Brown and Scholz, 1985; Brown, 1987; Wong et al., 1989; David et al., 1990; David, 1993; Brown et al., 1995; Brown and Bruhn, 1998; Zhu et al., 1995, 1999]. The characteristic types of pores of Wilcox shale, their contribution to anisotropic

transport properties, and their closure (and relaxation) upon cyclic loading are addressed elsewhere (O. Kwon et al., Permeability of Wilcox shale, 1, Anisotropy and mechanical path dependence on pore structure, submitted to *American Association of Petroleum Geologists Bulletin*, 2001, hereinafter referred to as Kwon et al., submitted manuscript, 2001). However, we still do not know enough about the microgeometries of pores or networks of connected pores in shale to improve upon the predictions of (6) or (7). In this paper, we focus on the determination of effective pressure for fluid flow in one orientation of shale, parallel to bedding, and determine the k - P_e relation adopting the cubic expression (6) for bedding-parallel flow.

3. Experimental Methods

Permeabilities of Wilcox shale to flow of 1 M NaCl solution parallel to bedding were determined by a transient pulse method [Brace et al., 1968; Sutherland and Cave, 1980; Trimmer, 1981]. Permeabilities parallel to bedding are higher than those perpendicular to bedding, and they show wider variation over the conditions that we imposed (Kwon et al., submitted manuscript, 2001); thus determinations of effective pressure and k - P_e relations for this orientation are superior to those for other orientations. For each permeability determination we imposed a step in fluid pressure at one end of a cylindrical specimen (25.4 mm long and 12.5 mm in diameter) and measured the time variation in the fluid pressure difference across its length. The effective pressure law for pore fluid flow was determined for selected samples of similar lithology using both the ratio-of-slope method [Walls and Nur, 1979; Bernabe, 1986, 1987] and the cross-plotting method [Walsh, 1981; David and Darot, 1989]. Paired permeability k and effective pressure P_e values were linearized according to the cubic law (6) and best fit, verifying the value of χ of the effective pressure law by iteration and minimizing variances in the k - P_e fit for different χ values. Assuming that all fitted parameters of (6) other than k_0 remain constant, the ability of the cubic law to characterize the nonlinear k - P_e relationship of Wilcox shale was tested using a larger permeability data set with samples of varying permeability (presumably associated with variations in porosity and lithology).

3.1. Starting Material

Specimens used in this study were prepared from shale core of the Wilcox formation recovered from a depth of ~3955 m in West Baton Rouge Parish, Louisiana (generously provided by R. R. Berg). The bottom hole temperature (121°C) was significantly greater than the dehydration temperature (~105°C) associated with the smectite-illite transition [Burst, 1969; Eberl and Hower, 1976]. The in situ pore pressure (63 MPa) for this interval (inferred from drilling mud weight) exceeded normal hydrostatic values observed elsewhere in the Gulf Coast [Dickinson, 1953; Schmidt, 1973], indicating a pressure difference between overburden and pore pressure of ~26 MPa. Clay mineral content of the core varies from 40 to 65% by volume. On the basis of X-ray diffraction of dehydrated and glycerated powder samples [Ibanez and Kronenberg, 1993], illite is the predominant clay mineral (29%) with lesser quantities of chlorite (14%), kaolinite (10%), and a trace of mixed layer illite-smectite (~2%); the remainder of the starting material consists of quartz (37%) and lesser quantities of pyrite, calcite, feldspar, and organics (8% combined). Samples selected for

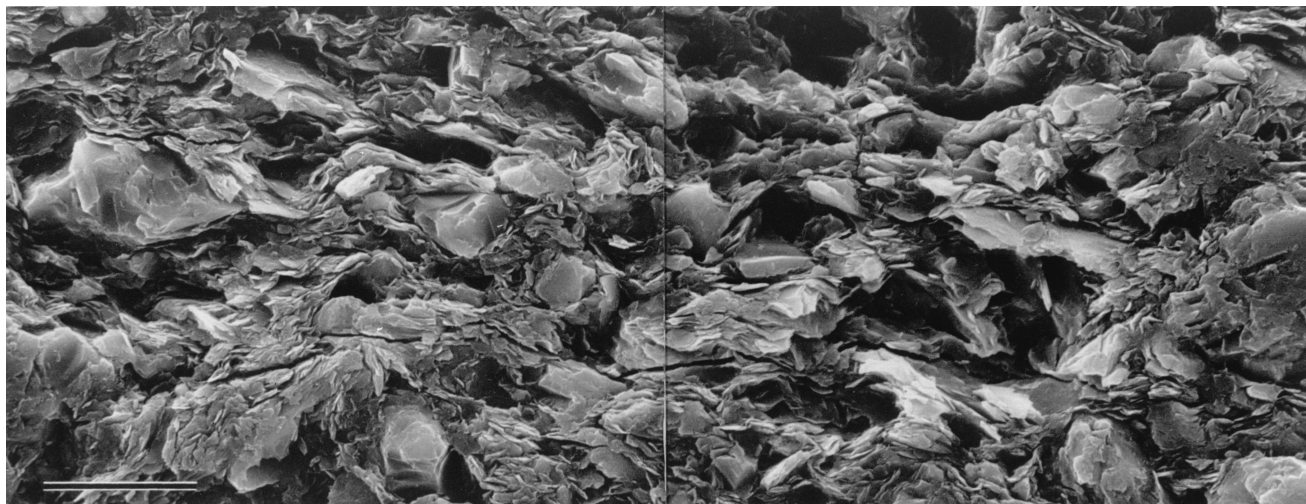


Figure 1. Secondary electron micrograph of Wilcox shale starting material (bedding parallel to long axis of figure). Clays form a contiguous matrix made up of clusters of clay grains with wavy basal (001) sheets subparallel to bedding; departures in (001) orientation correspond to nearby detrital quartz, feldspar, and pyrite. Pores of significance to fluid flow parallel to bedding include fine, grain-scale cleavage cracks within clustered clay minerals and intragranular, crack-like voids aligned parallel to bedding, all with high aspect ratios (bar scale is 10 μm long). Sample surface is treated with an aliphatic epoxy resin (Eponate 12, Pelco) and ground using 3- μm aluminum oxide powder.

this study were relatively low in clay content, ranging from 40 to 50%. No special procedures were followed to preserve the original pore fluid content of the core, and some modification of the clays and their surface hydration may have occurred as a result. Upon acquisition of the core we measured an initial water content of 2.1% (by weight loss upon heating representative material to 210°C). Specimens prepared for this study were diamond-cored, their ends ground parallel to each other (within $\sim 0.2^\circ$) and perpendicular to their cylindrical axes, and their connected pore space saturated by 1 M NaCl solution, adding ~ 2.7 wt % fluid to their original water contents.

Porosities measured from well logs range from 2.5 to 15% over the length of the core (records from Reese Oil and Gas Intra-coastal Land Co. well 2), with higher porosities corresponding to intervals of lower clay content. Connected porosities determined for cores used in this study range from 7 to 8 vol %, on the basis of weight gain following immersion in 1 M NaCl solution (density of 1040 kg/m³ [Wolf et al., 1979]). Bedding is expressed texturally (1) by compositional layering, with silty layers (<1 mm) of higher quartz content within a more clay-rich matrix, (2) by wavy, discontinuous clay mineral packets, and (3) by clay mineral alignments (Figure 1). Pores of varying geometry and character have been observed by electron microscopy and categorized according to their capacity as fluid conduits (Kwon et al., submitted manuscript, 2001). They include fine, grain-scale cleavage cracks within clustered clay minerals (with widths as small as a few nanometers and lengths of the order of the clay grain size) and intragranular, crack-like voids aligned parallel to bedding (with larger widths and lengths than the cleavage crack dimensions but with comparable aspect ratios).

Wilcox shale is similar in its clay mineralogy and porosity to Eleana argillite [Lin, 1978] and a shale from the Scotian shelf [Katsube et al., 1991] for which permeabilities have been measured. It has a porosity similar to Anita shale and a sandy mudstone which come from similar depths [Magara, 1978; Neglia, 1979], and it exhibits many of the textural features de-

scribed by Lee et al. [1985] and Kim et al. [1998] for deeply buried, well-consolidated shales. Further details regarding types of pores in Wilcox shale, their contribution to permeability anisotropy, and their response to cyclic loading are given by Kwon et al. (submitted manuscript, 2001). In addition, the sensitivity of permeability of this material to fluid composition has been investigated (O. Kwon et al., Permeability of Wilcox shale, 2, Influence of fluid chemistry on flow and functionally connected pores, submitted to *American Association of Petroleum Geologists Bulletin*, 2001), and mechanical properties are known from previous experimental studies of failure and deformation with fluids added and removed [Ibanez and Kronenberg, 1993; Kwon and Kronenberg, 1994].

Despite efforts to sample shale of uniform clay content and texture within a 1-m interval of the core, variations in permeability at a given effective pressure were observed that can be attributed to real variations in pore structure and reference permeability k_0 . Thus we determined the effective pressure law and the permeability-effective pressure relationship for Wilcox shale using a small subset of four selected samples. Three of these samples come from the same stratigraphic horizon, and one was chosen for its similar lithology and the fact that it displayed similar permeabilities at $(P_c - P_p) = 3$ MPa. The relationships determined for this subset were then tested, and variations in k_0 were evaluated using a larger set of permeability measurements.

3.2. Saturation and Pressurization

Samples were placed in heat-shrinkable polyolefin jackets with a thin coat of silicone applied to their cylindrical walls to form a seal to fluid flow between the sample and jacket. They were then immersed in a 1 M solution of NaCl over a period of >2 days, repeatedly applying a vacuum (>10 times) and bleeding atmospheric pressure back into the vacuum chamber to introduce as much fluid into pores of the sample as possible. Specimens were stored, immersed in NaCl solution until their jackets were sealed and pressurized and their permeability

measured. Layers of glass fiber felt were placed at both ends of each sample to ensure uniform access of pore fluid to the specimen ends, and pistons with pore pressure ports were placed at both ends, inserting them into the overlapping jacket. The seal between the pistons and jacket was accomplished by way of Nichrome wires, tied over a machined groove in each piston. Once the sample assembly was placed within the pressure vessel, the portion of the pore pressure system that required disassembly between experiments was placed under a vacuum for 30 min (to remove trapped air) and then filled with 1 M NaCl solution.

Once pore fluid was introduced, a confining pressure P_c of 3 MPa was applied. The fluid in contact with both specimen ends was then pressurized to $P_f = 2$ MPa (we distinguish P_f , the pressure measured in the pore pressure system, from P_p , the fluid pressure within specimen pores, as P_f may not equal P_p at first and equilibration may require significant times for low-permeability samples), holding P_c constant. Pore fluid was then bled from the system by cracking fittings repeatedly to ensure complete filling of the pore pressure system by the fluid and to achieve saturation of samples, as judged by the sensitivity of P_f to confining pressure P_c perturbations [Green and Wang, 1986]. Once P_f remained constant over 4–5 hours, it was considered at equilibrium with the internal pore pressure P_p of the sample. The amount of pore fluid added to samples upon increasing P_f was small compared with quantities previously added by vacuum impregnation ($\leq 3\%$ of that added by vacuum treatment), as judged by weight measurements made before and after experiments.

Confining and pore pressures were increased stepwise over an extended period of time to the desired experimental conditions, taking care that the difference between confining and pore fluid pressures did not exceed the ultimate value of $(P_c - P_p)$ at which permeability was to be measured. With increasing effective pressure, pores of weak solids may collapse irreversibly and previous measurements of shale (and clay aggregate) permeabilities show pronounced effects of load cycling, consistent with critical state stress-volume relations for soils [Schofield and Wroth, 1968; Olsen, 1972; Lin, 1978; Scott, 1980; Wood, 1990; Dewhurst et al., 1998; Kwon et al., submitted manuscript, 2001]. Once P_c and P_f remained constant at 3 and 2 MPa, respectively, P_c was increased by 2 MPa followed by an increment of 2 MPa in P_f , each time allowing 2–3 hours for pore pressure equilibration and repeating until the desired fluid pressure was reached. Once P_f was equal to the experimental, target pore pressure P_p and remained constant with time, confining pressure P_c was increased in 3-MPa steps, bleeding the pore fluid system as needed to maintain P_f and allowing ~ 1 hour for P_p equilibration. Once the target P_c was achieved, P_c was held constant and P_f monitored for 3–5 hours. Throughout, we assumed that internal values of pore pressure P_p were equal to the measured P_f if P_f remained constant over time; in the following, we refer to P_p when this criterion for equilibrium was satisfied.

Multiple measurements of permeability were made for each sample for increasing values of $(P_c - P_p)$. For ratio-of-slope determinations of the effective pressure law, P_c was increased sequentially (holding P_p constant), or P_p decreased (holding P_c constant) prior to each subsequent permeability measurement. For cross-plotting determinations of the effective pressure law, $(P_c - P_p)$ was increased, both by P_c increments and P_p decrements. Several samples were returned to $(P_c - P_p) = 3$ MPa before increasing $(P_c - P_p)$ further as part of

a study of cyclic loading on permeability (Kwon et al., submitted manuscript, 2001). These samples were unloaded to $(P_c - P_p) = 3$ MPa in steps of ≤ 3 MPa, either by reducing P_c or increasing P_p , and allowing 2–3 hours for pore pressure equilibration. Following this procedure, samples were again reloaded using the same protocol as described above. Measurements of permeability under decreasing P_c , effects of cyclic loading, and nonrecoverable reductions in pore space are not addressed in this paper, but we identify those measurements made after unloading and reloading, given that uncertainties in these measurements are somewhat larger than others due to P_c perturbations during this procedure.

3.3. Transient Pulse Experiments

Once the desired $(P_c - P_p)$ value was achieved, the upstream fluid pressure reservoir in contact with one specimen end was isolated from the downstream reservoir in contact with the opposite specimen end. The pressure in the upstream reservoir was then increased by an amount ΔP_i ($\leq 15\%$ of the initial P_p) using a piston-cylinder pressure generator (Figure 2a). Following the application of a fluid pressure difference across the sample, the pressure of the upstream fluid reservoir P_{up} was observed to decay, following an approximately log linear relationship with time (Figure 2b), and pressure of the downstream reservoir P_{dn} was observed to increase, both approaching a final equilibrium fluid pressure P_F by flow through the specimen. Both P_{up} and P_{dn} were measured to ± 0.02 MPa using high sensitivity pressure transducers (with resolution limited by an output measurement error of ± 0.01 mV). Daily fluctuations in ambient temperature (± 1 – 2°C) of the fluid reservoirs led to fluctuations in fluid pressure (± 0.08 MPa) greater than instrumental resolution. Temperature fluctuations of the pore pressure system were minimized by wrapping insulation around the fluid reservoirs and plumbing.

More importantly, we based our determinations of permeability on the decay of the fluid pressure difference across the specimen ($P_{up} - P_{dn}$) as a function of time. For any given transient pulse experiment the slope of $\log(\Delta P)$ versus t was essentially the same for $\Delta P = (P_{up} - P_{dn})$, $\Delta P = (P_{up} - P_F)$ and $\Delta P = (P_F - P_{dn})$. However, $\Delta P = (P_{up} - P_{dn})$ was much less sensitive to temperature fluctuation than the other ΔP values since both reservoirs experienced similar ambient temperature changes. To test that the observed reductions in pressure gradient across samples corresponded to flow through the sample (rather than to flow between the sample and jacket), fluid pressure stepping experiments were performed on an aluminum sample with the same silicone coat and jacket arrangement as used in the permeability experiments. These tests showed that the silicone provided an effective seal for confining pressures P_c that exceeded P_p by ≥ 0.5 MPa.

Fluid pressures in the upstream and downstream reservoirs were monitored until the difference between the two ($P_{up} - P_{dn}$) dropped below 40–50% of the initial pressure difference (ΔP_i) imposed at $t = 0$, and the data were fit by

$$(P_{up} - P_{dn}) = \Delta P_i e^{-\theta t} \quad (8)$$

to find θ (determined from the slope $-\theta/2.303$ in Figure 2b). Assuming that terms describing fluid storage within samples can be neglected [Brace et al., 1968; Sutherland and Cave, 1980], the value of θ can be expressed as

$$\theta = (kA/\eta\beta L)(1/V_{up} + 1/V_{dn}), \quad (9)$$

where k is permeability, A and L are the cross-sectional area and length of the sample, respectively, η is the absolute (dy-

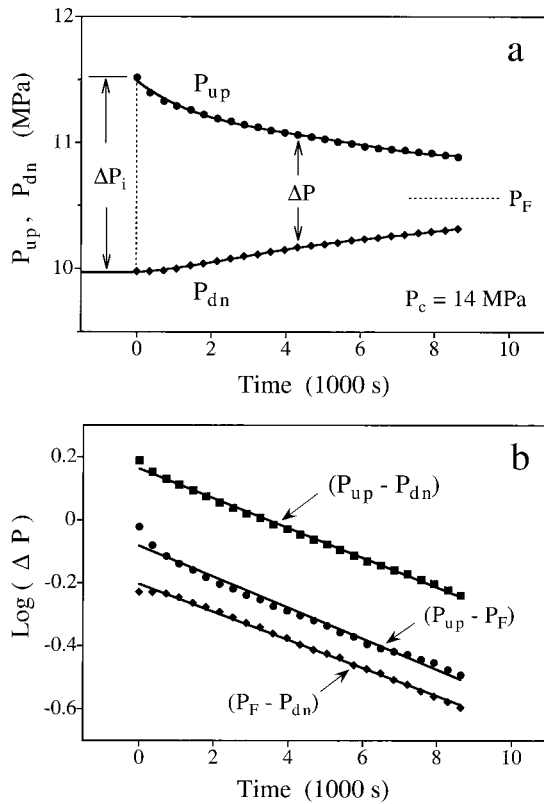


Figure 2. Transient pulse experiment used to determine permeability (WS22.11-2). (a) Raw fluid pressure in upstream reservoir P_{up} and fluid pressure in downstream reservoir P_{dn} versus time data. Prior to increasing P_{up} by ΔP_i (at $t = 0$), both P_{up} and P_{dn} were equal to P_f (which was taken to equal P_p within samples once P_f showed no variation with time). After applying the initial pressure difference ΔP_i across the sample length, P_{up} declines with time and P_{dn} increases, both approaching a new equilibrium fluid pressure P_F . ΔP shown is for $(P_{up} - P_{dn})$. (b) The same data recast as $\log(\Delta P)$ versus time, taking the difference between the upstream and final pressures ($P_{up} - P_F$), between the final and downstream pressures ($P_F - P_{dn}$), and between the upstream and downstream pressures ($P_{up} - P_{dn}$). The slopes in $\log(\Delta P) - t$ are the same for all measures of ΔP (within 5%), and each may be used to find θ (equation (8)), but scatter about best fit lines is minimum for $\Delta P = (P_{up} - P_{dn})$. Permeabilities k were determined from θ and equation (9).

dynamic) viscosity of the fluid, β is the compressibility of the fluid, and V_{up} and V_{dn} are upstream and downstream reservoir volumes, respectively. The viscosity of the NaCl solution at $\sim 20^\circ\text{C}$ was taken to be 1.1×10^{-9} MPa s [Wolf *et al.*, 1979]. Because of uncertainties in compressibility of 1 M solution of NaCl, its compressibility was assumed to be similar to that (4.56×10^{-4} MPa $^{-1}$) of water [Meyer *et al.*, 1979]. This could lead to an error in $kA/\eta BL$ of 10% [Millero *et al.*, 1977; Chen *et al.*, 1978; Lide, 1997]. Volumes of upstream (15.1 mL) and downstream (24.4 mL) reservoirs of the fluid pressure system were determined from their effective compressibilities after purging the system of air, isolating each reservoir, and imposing steps in pressure much like those in the permeability experiments. On the basis of these volumes and determinations of connected porosity for our samples, the ratio of sample pore volume to the upstream reservoir volume was 0.02, and that of the pore volume relative to the downstream reservoir was

0.013. Errors in permeability associated with fluid storage terms for these volume ratios are less than $\sim 1\%$ [Trimmer, 1981].

Uncertainties in permeability are dominated by real sample-to-sample variations in pore structure and, for individual samples, by variable reductions in pore space with the application of effective pressure. Observed variations in both fluid pressure measurements P_{up} , P_{dn} for individual transient pulse experiments correspond to ambient temperature fluctuations, but variations in the pressure difference ($P_{up} - P_{dn}$) are essentially equal (± 0.02 MPa) to instrumental error. On the basis of least squares fitting of $\log(P_{up} - P_{dn})$ versus time data [York, 1966], permeability k can be determined from the slope ($-\theta/2.303$) with a standard deviation of 1–3%, neglecting any errors in absolute reservoir volumes or values of fluid viscosity and compressibility. However, on the basis of departures of sequential permeability measurements (for individual samples) with increasing $(P_c - P_p)$ from values given by any chosen, smoothly varying function of k and $(P_c - P_p)$, uncertainties in permeability appear to be closer to $\pm 10\%$, presumably reflecting real variability in pore collapse. Samples that were unloaded from elevated $(P_c - P_p)$ values to 3 MPa and reloaded to the same or higher $(P_c - P_p)$ appear to show systematic reductions in k that fall within the observed $\pm 10\%$; however, determinations of k following unloading (and reloading) are of lower quality than measurements for samples that were not subjected to this procedure. Despite our efforts to limit effective pressures during load cycling to values below those of the previous maximum value achieved (at which compaction and pore collapse had occurred), additional nonrecoverable changes in porosity may have occurred during this procedure. Variations in permeability of $\pm 70\%$ were observed for samples taken from different stratigraphic horizons (all chosen for their similarity in clay content) and loaded to the same values of $(P_c - P_p)$.

Confining pressures P_c during the transient pulse measurements of k were controlled to within ± 0.2 MPa and measured within ± 0.06 MPa, leading to an uncertainty in reported values of $(P_c - P_p)$ of ± 0.07 MPa just before the upstream fluid pressure P_{up} was increased to impose a fluid pressure gradient. Once P_{up} was increased, however, true $(P_c - P_p)$ values (and P_e values) varied within the specimen, both spatially and temporally. Immediately after increasing P_{up} , $(P_c - P_p)$ values at the upstream sample end were reduced as much as 30% while $(P_c - P_p)$ at the opposite end was unchanged. During the course of each transient pulse experiment, $(P_c - P_p)$ in upstream portions of the sample increased with time as $(P_c - P_p)$ in downstream portions decreased, both approaching a final, equilibrium value somewhat smaller than the initial $(P_c - P_p)$.

Given that permeability of Wilcox shale is lower at higher $(P_c - P_p)$, we expect that bulk permeabilities determined for samples with axial gradients in $(P_c - P_p)$ are dominated by locally lower permeabilities where $(P_c - P_p)$ is higher. In addition, because (1) effective pressures throughout specimens (during each transient pulse measurement) were reduced from the initial, uniform value and (2) recoverable changes in k during unloading are smaller than nonrecoverable changes during loading [Lin, 1978; Dewhurst *et al.*, 1998; Kwon *et al.*, submitted manuscript, 2001], we do not expect that k increased much at the reduced values of $(P_c - P_p)$. On the basis of these considerations, we made no corrections to values of P_p or $(P_c - P_p)$ and simply report the values determined before P_{up} was increased.

Table 1. Permeability of Wilcox Shale Parallel to Bedding

Sample-Measurement	P_c , MPa	P_p , MPa	$P_c - P_p$, MPa	Permeability, $\times 10^{-21} \text{ m}^2$
<i>Measured at $P_p = 10 \text{ MPa}$</i>				
WS22.5-1	13	10	3	267.8 (± 1.2)
WS22.7-1	13	10	3	218 (± 3.2)
WS22.11-1	13	10	3	186.2 (± 1.7)
WS22.25-1	13	10	3	288.2 (± 2.8)
WS22.11-2	14	10	4	113.6 (± 0.9)
WS22.5-2	15	10	5	89.9 (± 0.8)
WS22.7-2	15	10	5	101.4 (± 1.9)
WS22.11-3	15	10	5	77.6 (± 0.9)
WS22.11-5 ^a	15	10	5	64.2 (± 0.9)
WS22.11-7 ^a	15	10	5	62.1 (± 0.6)
WS22.11-8	16.5	10	6.5	24.3 (± 0.2)
WS22.5-3	18	10	8	29.6 (± 0.2)
WS22.7-3	18	10	8	55.9 (± 0.7)
WS22.11-9	18	10	8	11.4 (± 0.2)
WS22.10-1	18	10	8	16.7 (± 0.6)
WS22.10-2	19	10	9	9.22 (± 0.2)
WS22.10-3	20.5	10	10.5	3.67 (± 0.1)
WS22.10-4	22	10	12	3.22 (± 0.1)
<i>Measured at $P_c = 22 \text{ MPa}$</i>				
WS22.12-1	22	19	3	189.8 (± 1.9)
WS22.12-2	22	18	4	129.4 (± 0.7)
WS22.12-3	22	17	5	94.6 (± 1.6)
WS22.12-5 ^b	22	15.5	6.5	55.8 (± 0.3)
WS22.12-7 ^b	22	14	8	27.4 (± 0.1)
WS22.12-9 ^b	22	13	9	11.3 (± 0.2)
WS22.12-11 ^b	22	11.5	10.5	5.1 (± 0.1)
WS22.12-12	22	10	12	3.64 (± 0.1)
<i>Measured at $P_c = 35 \text{ MPa}$</i>				
WS22.40-1	35	32	3	168.6 (± 3.2)
WS22.40-4	35	31	4	93.9 (± 1.8)
WS22.40-5	35	30	5	63.7 (± 0.8)
WS22.40-8	35	28.5	6.5	31.2 (± 0.2)
WS22.40-9	35	27	8	22.4 (± 0.1)
WS22.40-12	35	26	9	15.9 (± 0.1)
WS22.40-13	35	23	12	11.7 (± 0.1)
<i>Measured at $P_c = 45 \text{ MPa}$</i>				
WS22.40-2	45	42	3	150.2 (± 3.6)
WS22.40-3	45	41	4	121.7 (± 2.7)
WS22.40-6	45	40	5	57.2 (± 0.9)
WS22.40-7	45	38.5	6.5	42.1 (± 0.4)
WS22.40-10	45	37	8	23.1 (± 0.2)
WS22.40-11	45	36	9	21.4 (± 0.3)
WS22.40-14	45	33	12	12.1 (± 0.1)

^aSample returned to $(P_c - P_p) = 3 \text{ MPa}$ by decreasing P_c at constant $P_p = 10 \text{ MPa}$ and then repressurized to specified P_c (and specified value of $P_c - P_p$) prior to measurement of tabulated permeability.

^bSample returned to $(P_c - P_p) = 3 \text{ MPa}$ by increasing P_p at constant $P_c = 22 \text{ MPa}$ and then applying specified value of $(P_c - P_p)$ by decreasing P_p prior to measurement of tabulated permeability.

4. Results

Permeabilities measured parallel to bedding are assembled in Table 1, organized according to the values of confining pressure P_c and pore pressure P_p imposed. Samples WS22.10, WS22.11, and WS22.12, taken from the same stratigraphic interval of the core, and sample WS22.40, prepared from core just 0.2 m away, exhibit a wide range of permeabilities depending on the confining and pore pressures that they were subjected to. Together, these samples were used to determine the effective pressure law and the permeability–effective pressure relationship, assuming that they have the same clay content, porosity, and reference permeability k_0 . Several transient pulse experiments were performed for each sample, as indicated by the sequence number following the hyphen in each sample-measurement entry in Table 1. Measurements follow-

ing an unloading cycle to $(P_c - P_p) = 3 \text{ MPa}$ are identified according to whether P_c was dropped or P_p increased. Samples WS22.5, WS22.7, and WS22.25 were taken within the same 1-m length of core as the others; however, their permeabilities are more variable. Errors in tabulated permeabilities represent the standard deviation in slope θ determinations, while error bars shown in the figures represent larger uncertainties due to real variations in connected pore space and sample-to-sample variation.

4.1. Effective Pressure

At constant pore pressure ($P_p = 10 \text{ MPa}$), permeabilities measured for samples WS22.10 and WS22.11 drop by 2 orders of magnitude (from $1.9 \times 10^{-19} \text{ m}^2$ to $3.2 \times 10^{-21} \text{ m}^2$) as confining pressure P_c is increased (from 13 to 22 MPa), in-

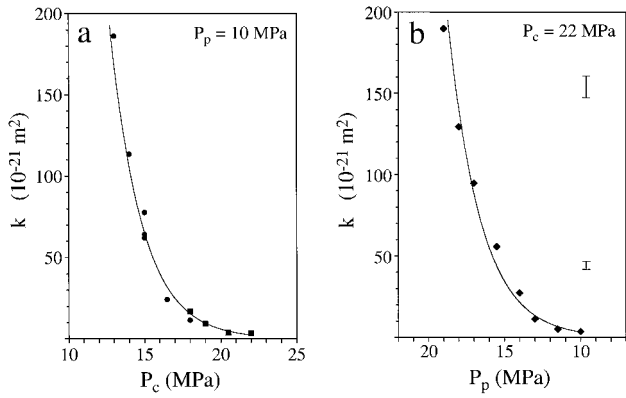


Figure 3. Permeability k as a function (a) of P_c at constant $P_p = 10$ MPa and (b) of P_p at constant $P_c = 22$ MPa for samples prepared from the same stratigraphic horizon. Multiple measurements for sample WS22.11 with increasing P_c are shown as solid circles, while those of WS22.10 are shown as solid squares. Permeability measurements for sample WS22.12 were made at decreasing P_p , shown as solid diamonds. Error bars shown are significantly greater than instrumental uncertainty and represent observed scatter in k values between separate measurements for the same sample. Ascending values of P_p along the axis of Figure 3b are shown reversed, so that effective pressure increases to the right.

creasing ($P_c - P_p$) by a factor of 4 (Figure 3a). Similarly, permeabilities measured for WS22.12 drop (from 1.9×10^{-19} m² to 3.6×10^{-21} m²) as pore pressure P_p is decreased, and ($P_c - P_p$) is increased over the same range (Figure 3b). The ratio-of-slope method of determining the effective pressure law is based on comparing the sensitivities of the physical property, k in our study, to confining pressure and to pore pressure [Walls and Nur, 1979; Bernabe, 1987]. Irrespective of the form of the permeability-pressure relationship $k(P_e)$, χ may be determined by examining derivatives of k with respect to P_c and P_p at a given value of k . In order to apply this method using all of our data for WS22.10, WS22.11, and WS22.12, we plot $\log k$ versus P_c (Figure 4a) and $\log k$ versus P_p (Figure 4b), making the choice of axes on a strictly pragmatic basis, without asserting that the permeability-pressure relationship is strictly exponential. While highly empirical, this approach leads to well-defined slopes ($\partial \log k / \partial P_c$) _{P_p} = $-0.209 (\pm 0.010)$ and ($\partial \log k / \partial P_p$) _{P_c} = $0.203 (\pm 0.011)$ over the ranges of P_c and P_p explored and over all k measured, yielding

$$\begin{aligned} \chi &= -(\partial \log k / \partial P_p) / (\partial \log k / \partial P_c) \\ &= 0.97 (\pm 0.07) \end{aligned} \quad (10)$$

remarkably close to unity.

Permeabilities of samples WS22.12 and WS22.40 were measured over comparable ranges at three values of P_c (22, 35, and 45 MPa), varying P_p at each P_c (Figure 5). The cross-plotting method of determining the effective pressure law is based on determining the relative importance of P_c and P_p to the value of k by plotting P_c versus P_p at constant k and determining the slope χ [Walsh, 1981; David and Darot, 1989]. Since k is not experimentally controlled as the independent variable, we could not measure P_p at constant k and P_c directly to generate a $P_c - P_p$ cross plot. However, by fitting the $k - P_p$ data for each value of P_c (again, by a simple exponential function) and finding the interpolated values

of P_p at constant k and P_c (dashed lines, Figure 5a), we generated isopermeability contours in terms of P_c and P_p (Figure 5b). Best fit values of χ vary about one, and the mean $\chi = 0.99 (\pm 0.06)$ is identical within error to its value determined by the ratio-of-slope method. Together, these results show that the effective pressure law for the permeability of Wilcox shale is indistinguishable from Terzaghi's [1923, 1925] original expression.

4.2. Permeability: Effective Pressure Relation

The same data selected to determine effective pressure P_e were used to determine the dependence of k upon P_e . Adopting (6) and iterating over χ , the data were recast in terms of k/k_0 and P_e [Gangi, 1978] that can be fit by simple linear regression (Figure 6), yielding best fit parameters

$$k_0 = \sim 10^{-17} \text{ m}^2$$

$$m = 0.159 (\pm 0.007)$$

$$P_1 = 19.3 (\pm 1.6) \text{ MPa}$$

for $\chi = 0.99$ to 1.00, where m is the slope in $\log [1 - (k/k_0)^{1/3}]$ versus $\log P_e$ and the intercept equals $-m \log P_1$. Because a rigorous seal between samples and jackets was not possible using our experimental techniques at $(P_c - P_p) < 0.5$ MPa, we made measurements of k only at $(P_c - P_p) \geq 3$ MPa. Thus the reference permeability k_0 (defined at $P_e = 0$) is not well determined. Comparisons of fits to the data for varying k_0 indicate that k_0 must exceed 10^{-18} m², but fits to the data for larger k_0 are of similar quality. Improvement on our order-of-magnitude estimate of k_0 would require permeability measurements at lower P_e or specimens that show less scatter in k . Despite this difficulty, values of parameters m and P_1 are insensitive to the value of k_0 , and our ability to infer values of k at high effective pressures is much better than our ability to predict k at $P_e < 3$ MPa. By examining the quality of fit of the cubic $k - P_e$ relation to our data for varying χ , we obtained yet another determination of χ equal (or nearly equal) to 1, in confirmation of the ratio-of-slope and cross-plotting analyses.

In our determination of the permeability-effective pressure relation we assumed that the samples that we selected had identical transport properties. Yet residuals of the data from

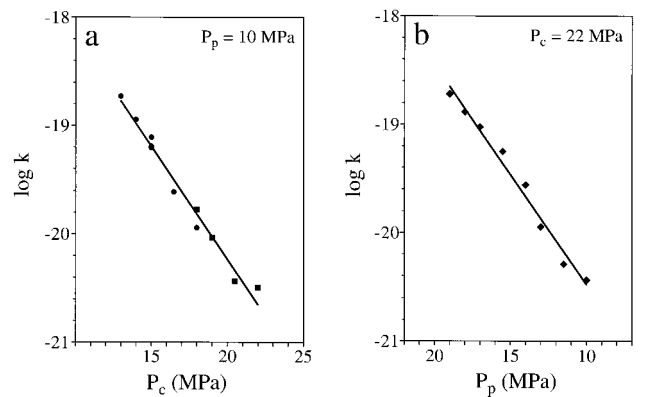


Figure 4. Permeability data linearized by taking the logarithm of k and plotting (a) against P_c at constant P_p , and (b) against P_p at constant P_c to determine the effective pressure coefficient χ by the ratio-of-slope method. P_p scale along abscissa of Figure 4b is shown reversed. Data for samples WS22.10, WS22.11, and WS22.12 are shown as solid squares, circles, and diamonds, respectively.

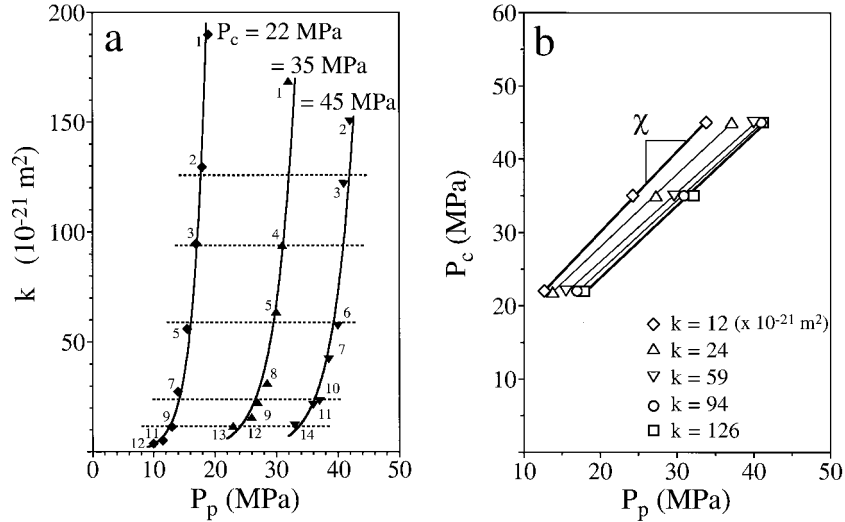


Figure 5. Determination of effect pressure law using the cross-plotting method. (a) Permeability k versus pore pressure P_p measured at constant P_c values of 22, 35, and 45 MPa. Permeabilities of sample WS22.12 at $P_c = 22$ MPa (same as in Figure 3b) are shown as solid diamonds, and permeabilities measured for sample WS22.40 at $P_c = 35$ and 45 MPa are shown as solid triangles. The sequence of permeability measurements is given by numbers next to data (measurements 4, 6, 8, and 10 for sample WS22.12 are not shown as these were made upon unloading to $P_c - P_p = 3$ MPa). Dashed lines indicate values of k chosen to construct Figure 5b. (b) Cross plot of P_c versus P_p . The slopes of isopermeability contours (defined by best fit data) in the $P_c - P_p$ plane yield values of the effective pressure coefficient χ (k values of open symbols given).

the best fit relation are not small (Figure 6), and larger deviations are apparent when the best fit relation is compared with permeabilities of the remaining samples (Table 1). However, if we allow the reference permeability k_0 of each sample to vary, assuming that m and P_1 are the same for all, much better fits are accomplished. Plotting permeability of all measured samples (Table 1), normalizing by reference permeabilities k_0 in-

dividually fit for each sample, the cubic law (6) with constant m and P_1 appears to describe the results well for our entire data set (Figure 7), even when the logarithm of k/k_0 is not taken. Real sample-to-sample variations suggested by this analysis are of the order of 70%, even though samples were of comparable clay content; larger variations in k_0 are expected for samples of more variable lithology and porosity.

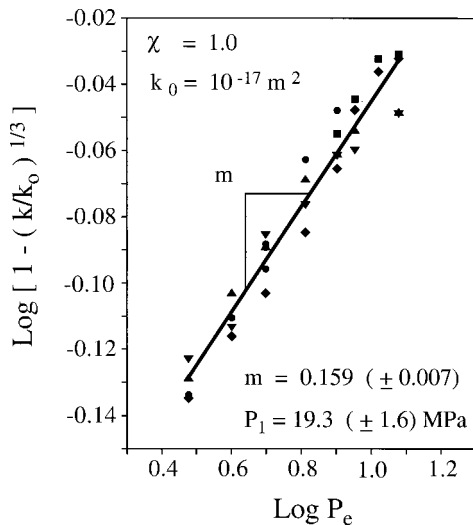


Figure 6. Permeability-effective pressure relation determined for the same selected data set used to determine effective pressure law, plotting k/k_0 and $P_e (= P_c - P_p)$ in terms according to the modified cubic law (6). The slope of the data yield the value of m and the intercept is equal to $-m \text{ log } P_1$. Solid squares (WS22.10), circles (WS22.11), diamonds (WS22.12), and triangles (WS22.40) are the same data as in Figures 3 to 5.

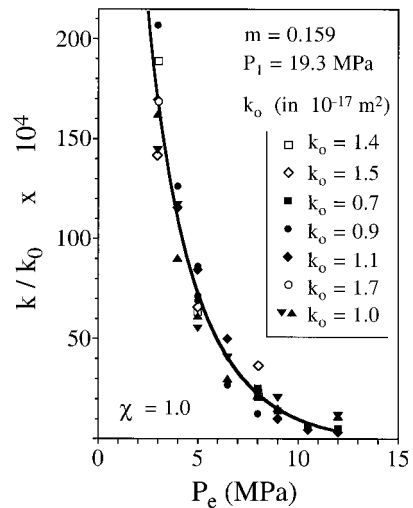


Figure 7. Permeabilities of entire data set of Table 1, normalized by reference permeabilities k_0 determined for each sample versus effective pressure P_e , compared with the cubic law (6) determined for selected data, assuming m and P_1 are constants (and do not vary among samples). Solid symbols represent the same measurements as presented in Figures 3–6. Data for samples WS22.5, WS22.7, and WS22.25 are shown as open squares, diamonds, and circles, respectively.

5. Discussion

The range of permeabilities (2.9×10^{-19} to 3.2×10^{-21} m²) measured for flow parallel to the bedding of Wilcox shale is well within the range previously reported for other shales and mudstones [Young *et al.*, 1964; Lin, 1978; Magara, 1978; Bredehoeft *et al.*, 1983; Katsube *et al.*, 1991; Schlomer and Krooss, 1997; Dewhurst *et al.*, 1998, 1999]. Permeability is strongly influenced by confining and pore pressures, with values approaching our lower threshold for measurement ($\sim 10^{-21}$ m²) at an effective pressure P_e of just 12 MPa. The effective pressure P_e for shales and mudstones has commonly been assumed to equal the difference between confining and pore pressures ($P_c - P_p$). Our determination of the effective pressure coefficient $\chi = \sim 1$ for permeability of Wilcox shale supports this assumption. Furthermore, it suggests that fractional areas of contact that govern physical properties [Gangi and Carlson, 1996] are small for well-consolidated shales, much as they are for uncemented soils or fractured rocks [Terzaghi, 1925; Hubbert and Rubey, 1959; Handin *et al.*, 1963].

5.1. Implications for Fluid Conduits

The fit of the modified cubic law (6) to the measured permeability–effective pressure data (Figure 7) is consistent with microstructural observations (Figure 1), which show that pores capable of transmitting fluid parallel to bedding are crack-like in geometry. Of the parameters determined, k_0 is the least constrained by our data set and P_1 is the most constrained. Determination of k_0 ($\sim 10^{-17}$ m²) could be improved by making measurements at lower P_e (preferably at the reference state $P_e = 0$). However, this parameter incorporates the complexity of the entire network of pores, and real variations of $\sim 70\%$ are apparent among samples. The value of m shows some covariance with k_0 . Nevertheless, it is reasonably well determined for a given k_0 , and the best fit value of m ($= 0.159$) is well within permissible values ($0 < m < 1$) of the asperity model upon which (6) is based [Gangi, 1978]. The corresponding power law exponent n ($= 1/m$) describing the asperity height distribution is large ($n = \sim 6$); thus the conduits that govern permeability are predicted to have rough, poorly mated opposing surfaces.

We are confident in our determination of P_1 ; its best fit value is insensitive to uncertainties in k_0 and m . However, as an effective modulus of asperities, P_1 ($= 19.3$ MPa) is remarkably small. Bulk moduli κ of clay-rich shales determined from velocity measurements range from 10 to 39 GPa [Han *et al.*, 1986; Johnston, 1987; Vernik and Nur, 1992; Hornby, 1994; Johnston and Christensen, 1995; Vernik and Liu, 1997], while effective κ values determined from the static pressure-volume response of shales are in the range 1–4 GPa [Johnston, 1987; Swan *et al.*, 1989]. On the basis of volume changes in response to increases in mean stress (O. Kwon and A. K. Kronenberg, Failure strength of Wilcox shale: Effects of pore fluid, volume change, and strain rate, submitted to *Tectonophysics*, 2001), we estimate an apparent drained κ for Wilcox shale upon first loading of ~ 3 GPa. By comparison with any of these macroscopic measures of the material bulk modulus, $P_1 < 10^{-2} \kappa$.

Nonlinear pressure-volume response and increases in apparent stiffness of shales and clay aggregates with cyclic loading [Braddock and Machette, 1976; Karig and Hou, 1992; Olgaard *et al.*, 1995] indicate that inelastic processes are responsible for much of the volume reduction as P_e is increased. Thus macroscopic, static values of κ are well below acoustically deter-

mined values, and they are well below the intrinsic moduli of the solid phases. Likewise, we suspect that the low value of P_1 is explained by inelastic distortions of asperities. With increasing P_e , pore geometries change, and any changes in width-to-height ratios of loaded asperities are expected to increase the value of P_1 . Thus, while we determine just one value for P_1 in our fitting procedure, P_1 is likely to be a function of P_e . Indeed, without such increases in P_1 , P_e of geologically reasonable magnitudes may exceed our best fit value of P_1 (determined for $3 \leq P_e \leq 12$ MPa), resulting in predicted values of k that are negative. Instead, we expect that P_1 increases substantially as P_e is increased, always maintaining a ratio $P_e/P_1 < 1$ and leading to less dramatic decreases in k at high P_e than predicted by the cubic law with constant P_1 .

The measured permeabilities can be fit equally well by Walsh's [1981] relationship (7) with reference permeability $k_0 = 1.74 \times 10^{-19}$ m² at $P_0 = 3$ MPa and $(2^{1/2} h/a_0) = 0.508$. Over the range of measurements, residuals between the data and the best fit relationships (6) and (7) are virtually identical, as might be expected by the similarity of the models used to derive these expressions. Moreover, without changes in asperity dimensions (h/a_0), expression (7) also predicts non-physical values of k at high P_e ; for k to remain positive at all P_e , values of $(2^{1/2} h/a_0)$ must decrease with increasing P_e .

The functional dependence of k upon increasing effective pressure for Wilcox shale appears to be uniform among samples, and observed sample-to-sample variations in k can be explained by differences in k_0 (Figure 7). The modified cubic law applied in this study is also capable of describing the nonlinear k - P_e relations reported for other shales, mudstones, and clay aggregates [Lin, 1978; Morrow *et al.*, 1984; Katsube *et al.*, 1991; Vasseur *et al.*, 1995; Dewhurst *et al.*, 1999]. However, the ranges of k_0 (from 2×10^{-20} to 5×10^{-15} m²), m (from 0.03 to 0.32), and P_1 (from 19 to 640 MPa) among materials of widely varying lithology and porosity are large.

Substantial differences in k_0 can readily be explained by variations in clay content and connected pore space [Katsube *et al.*, 1991; Dewhurst *et al.*, 1998, 1999]. Even for Wilcox shale samples selected for their uniformity, we find that k_0 varies. Variations in m , however, may reflect finer-scale variations in pore apertures and roughness of fluid conduits, as described by asperity height distributions. P_1 values best fit to the permeabilities reported for these same argillaceous rocks (and aggregates) vary by over an order of magnitude. While these materials differ greatly in lithology and texture, observed variations in P_1 do not require any differences in moduli of clay minerals (or other phases) making up asperities of fluid conduits. Instead, P_1 values correlate with the effective pressures at which permeabilities were measured. The most comparable P_1 value ($= 28$ MPa for Eleana argillite) to ours is given by permeabilities measured at $3 \leq P_e \leq 24$ MPa [Lin, 1978] and the largest P_1 ($= 430$ and 450 MPa) is given by permeabilities (of kaolinite and illite aggregates, respectively) measured at $30 \leq P_e \leq 200$ MPa [Morrow *et al.*, 1984]. We propose that systematic variations in P_1 with P_e are due to inelastic changes in loaded asperity dimensions.

5.2. Influence of Clay Distributions

Values of χ for permeability of sandstones and sand aggregates consisting of $\geq 99\%$ quartz are ≤ 1 [Zoback and Byerlee, 1976; Walls and Nur, 1979; David and Darot, 1989], much as the coefficient χ determined in this study for shale. However, χ values reported for clay-bearing sandstones exceed 1 (Figure

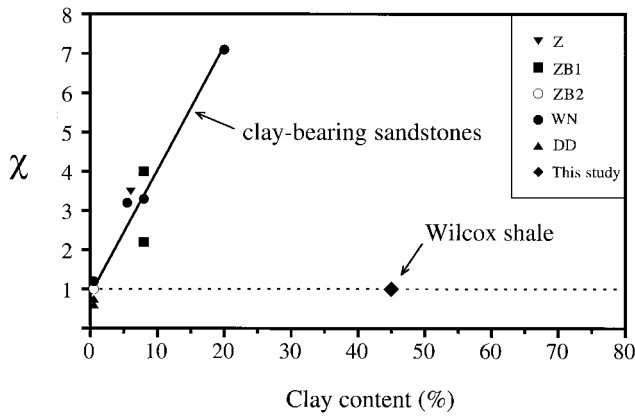


Figure 8. Effective pressure law coefficient χ versus clay content for sandstones and Wilcox shale, drawing on data of *Zoback* [1975], *Zoback and Byerlee* [1975, 1976], *Walls and Nur* [1979], and *David and Darot* [1989] (labeled Z, ZB1, ZB2, WN, and DD, respectively). Sandstones display an apparent trend of increasing χ with increasing clay content, with χ reaching 7.1 at a clay content of 20%, while Wilcox shale exhibits $\chi = 1$ for a clay content of 40–50%.

8), with an apparent correlation between χ and clay mineral content [*Zoback*, 1975; *Zoback and Byerlee*, 1975, 1976; *Walls and Nur*, 1979]. Values of χ as great as 7.1 for a clay content of

20% indicate that P_p has a significantly greater effect on permeability than P_c , a result that is difficult to reconcile with poroelastic models leading to equations (2)–(4) [*Biot*, 1941; *Biot and Willis*, 1957; *Skempton*, 1961; *Nur and Byerlee*, 1971; *Robin*, 1973; *Garg and Nur*, 1973; *Berryman*, 1992; *Gangi and Carlson*, 1996]. For porous media with homogeneous elastic properties, χ must be less than unity given that κ , the modulus of the rock, is less than κ_s , the intrinsic modulus of the solid (or that A_c , the true area of loaded contacts, is less than A , the total area).

In order to explain their unusual permeability results for Berea sandstone, *Zoback and Byerlee* [1975] proposed a microstructural model of a composite porous solid consisting of quartz grains that form a rigid load-supporting framework and clay minerals lining the connected pore space. Simplifying their conceptual model to nested hollow cylinders loaded externally by P_c and internally by P_p (Figure 9), *Zoback and Byerlee* [1975] considered the sensitivities of fluid conduit dimensions to applied pressures P_c and P_p when the compressibility of the outer quartz cylinder is low and the compressibility of the inner clay cylinder is high. In contrast to the behavior of a porous medium made up of just one solid (Figures 9a and 9d), the outer, stiffer cylinder of the composite may disproportionately support external loads leading only to small volumetric strains throughout, while the inner more compliant cylinder may experience large strains associated with changes in P_p without requiring large strains in the outer cylinder (Figures 9b and 9c

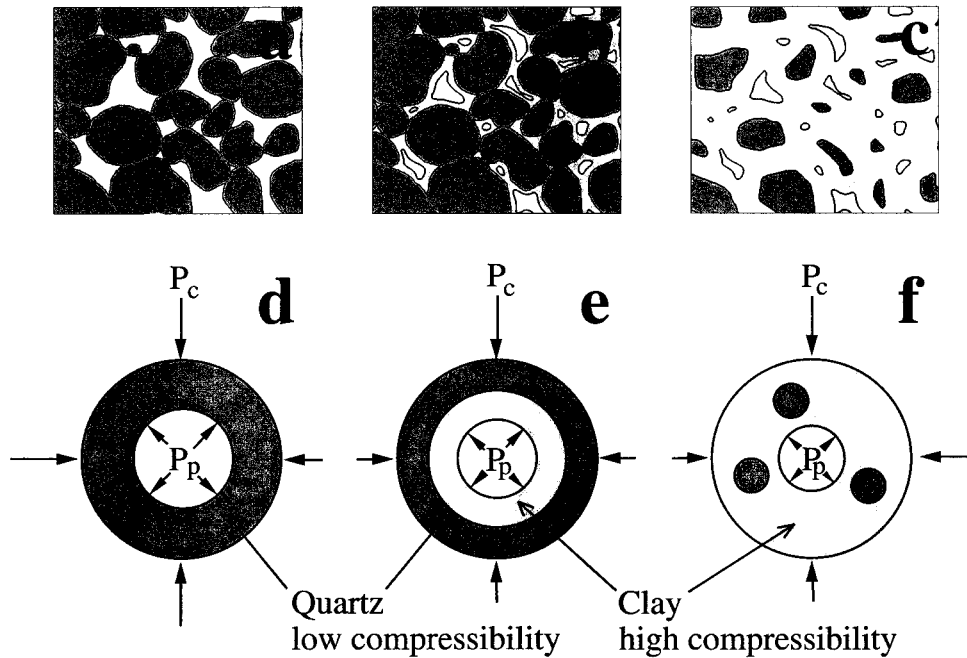


Figure 9. Phase distributions and effective pressure laws for porous media made up of two solids, such as quartz and clay minerals with low and high compressibilities, respectively, to confining pressure P_c and pore pressure P_p . Schematic microstructures of (a) pure quartz sandstones, (b) clay-bearing sandstones in which clays line the pores, and (c) shales and mudstones with high clay contents, with (d, e, and f) corresponding models simplified to reveal the sensitivity of fluid conduit dimensions to externally applied P_c and internally applied P_p (adapted after *Zoback and Byerlee* [1975]). For single-phase aggregates such as pure quartz sandstones (Figures 9a and 9d), $\chi \leq 1$ is predicted by equations (2)–(4). For sandstones made up of a strong stress-supporting framework quartz and high-compressibility clays lining pores (Figures 9b and 9e), fluid conduit dimensions may be influenced more strongly by P_p than P_c with the result that $\chi \geq 1$. For clay-rich shales and mudstones, clays form a connected matrix and conduit dimensions are similarly affected by P_c and P_p , resulting in $\chi \leq 1$.

9e). Thus changes in fluid conduit dimensions in response to changes in P_c may be small, while changes in these dimensions in response to changes in P_p may be substantial. *Berryman* [1992, 1993] developed this model further and solved explicitly for the dependence of χ upon the elastic properties of more general porous aggregates made up of two solids. Success of this model in predicting large χ values depends critically upon local pore compressibilities that are large relative to macroscopic aggregate compressibilities. The spatial distribution of clays relative to pores remains critical. Although experimental tests of these models and their dependence on clay distributions are still needed, permeabilities of sandstones are known to vary with clay distribution [Howard, 1992].

The results of this study for Wilcox shale show that the trend of increasing χ with increasing clay content, as displayed by sandstones, must fail at some threshold in clay content (Figure 8) between 20 and 40%. Scanning electron microscope observations of Wilcox shale show that clay minerals are highly contiguous, and we propose that the threshold between anomalously large χ values and normal values ≤ 1 corresponds to that point at which clays make up a connected matrix. Once quartz grains and other low-compressibility phases are isolated, and the applied P_c is supported by a compliant clay matrix, changes in conduit dimension (Figures 9c and 9f) associated with changes in both P_c and P_p will be governed by properties of the same solid, and we expect values of $\chi \leq 1$.

5.3. Geological Implications

Permeabilities measured for shales are many orders of magnitude smaller than those reported for sandstones, and their occurrence may define stratigraphic horizons that serve as pressure seals and divide reservoirs into fluid compartments [Bredhoeft and Hanshaw, 1968; Bradley, 1975; Hunt, 1990; Deming, 1994]. In the absence of capillary effects related to nonwetting hydrocarbons, shale layers 100 to 1000 m thick must have permeabilities $\leq 10^{-22}$ to 10^{-24} m² to seal against fluid transport over geologic times (≥ 10 Myr) and gradients in head [Deming, 1994]. While few laboratory measurements of permeability reach such low values, the pronounced effect of P_e on permeability of Wilcox shale (and other argillaceous rocks) indicates that permeabilities at geologically reasonable values of P_e are sufficiently small to prevent significant subsurface fluid flow. Our ability to extrapolate the fitted cubic law for Wilcox shale to high P_e values is limited by the constant value of P_1 determined over $3 \leq P_e \leq 12$ MPa. Nevertheless, if we use the cubic law to predict k at $P_e = 18$ MPa, just 50% greater than the highest value imposed in our experiments, k values for Wilcox shale drop to $\sim 10^{-23}$ m².

Thin shale layers may not form seals to fluid transport over geologic times. However, shale layers interbedded with siltstones or highly permeable sandstone layers may impart an apparent anisotropy to fluid transport properties, as expressed by large-scale flow parallel to and perpendicular to bedding. In cases where shales and clay-bearing sandstones are finely interbedded, particularly interesting predictions are made by their contrasting effective pressure laws. Given that neighboring shales and clay-bearing sandstones at comparable P_c reach equilibrium with respect to pore pressure P_p , effective pressures governing their permeabilities must be different. Effective pressures may even be positive in shale layers while P_e is negative in clay-bearing sandstones. As an example, effective pressures within neighboring shale and clay-bearing sandstone layers with $\chi = 1$ and 4, respectively, are predicted to equal 10

and -20 MPa at common equilibrium values of $P_c = 20$ MPa and $P_p = 10$ MPa.

6. Conclusions

Permeabilities of Wilcox shale measured parallel to bedding at varying confining and pore pressures confirm that argillaceous strata of sufficient thickness may serve as pressure seals capable of maintaining gradients in head and abnormal fluid pressures over geologic times. From experimental measurements made on selected samples under sequentially increasing $(P_c - P_p)$ and comparisons with permeabilities reported for other shales and clay-bearing sandstones, we conclude the following:

1. Permeability of shale depends on P_c and P_p with remarkably similar sensitivities, with an effective pressure coefficient $\chi (= 0.99 \pm 0.06)$ that is indistinguishable from 1; $P_e = P_c - P_p$.
2. The dependence of permeability k upon effective pressure P_e may be described by a simple cubic law $k = k_0[1 - (P_e/P_1)^m]^3$; for Wilcox shale, parameters $k_0 = \sim 10^{-17}$ m², $m = 0.159$, and $P_1 = 19.3$ MPa describe flow parallel to bedding at $3 \leq P_e \leq 12$ MPa, presumably through fine, crack-like conduits. Reference permeabilities k_0 of differing shales, mudstones, and clay aggregates vary substantially and appear to be sensitive to clay content, porosity, and tortuosity. Values of m for Wilcox shale and other argillaceous rocks are small, reflecting rough, poorly mated conduit surfaces. The value of P_1 for Wilcox shale is small relative to elastic bulk moduli, and it probably represents the inelastic distortions of conduit surface asperities. P_1 is expected to increase with increasing applied P_e .
3. The effective pressure law for Wilcox shale is in contrast to effective pressure laws reported for the permeabilities of clay-bearing sandstones. Large values of $\chi > 1$ for these sandstones appear to require a load-supporting framework of quartz or other low-compressibility phases and heterogeneous distributions of compliant clays relative to pore space. The trend of increasing χ with increasing clay content exhibited by sandstones is expected to break down at clay contents between 20 and 40% once clays are contiguous throughout the rock and support externally applied P_c as well as P_p . Differing effective pressure laws for rocks of variable clay content and texture also suggest that transport properties and the effective pressures governing them differ for thinly interbedded shales and clay-bearing sandstones at common, equilibrium values of P_c and P_p .

Acknowledgments. Many thanks go to Robert Berg, Richard Carlson, and David Wiltchko for helpful discussions and to Doug Schmitt, Mark Zoback, and an anonymous reviewer for their constructive criticism. We'd prefer to thank Mel Friedman in the same manner, as his questions and comments helped initiate this work. Sadly, though, Mel died unexpectedly on March 11, 1997, and we must acknowledge discussions with him in memory of him. We are thankful to Robert Berg for generously providing the Wilcox shale core for use in this study. As always, we benefited from the technical support and experience of Jackie Magouirk. This study was supported by a grant from the U.S. Department of Energy (grant DE-FG05-87ER13711); their support is gratefully acknowledged.

References

- Addis, M. A., and M. E. Jones, Volume changes during diagenesis, *Mar. Pet. Geol.*, 2, 241–246, 1985.

- Banthia, B. S., M. S. King, and I. Fatt, Ultrasonic shear-wave velocities in rocks subjected to simulated overburden pressure and internal pore pressure, *Geophysics*, 30, 117–121, 1965.
- Bennett, R. H., K. M. Fischer, D. L. Lavoie, W. R. Bryant, and R. Rezak, Porometry and fabric of marine clay and carbonate sediments—Determinants of permeability, *Mar. Geol.*, 89, 127–152, 1989.
- Berg, R. R., and M. F. Habeck, Abnormal pressures in the lower Vicksburg, McAllen ranch fields, south Texas, *Trans. Gulf Coast Assoc. Geol. Soc.*, 32, 247–253, 1982.
- Bernabe, Y., The effective pressure law for permeability in Chelmsford granite and Barre granite, *Int. J. Rock Mech. Min. Sci.*, 23, 267–275, 1986.
- Bernabe, Y., The effective pressure law for permeability during pore pressure and confining pressure cycling of several crystalline rocks, *J. Geophys. Res.*, 92, 649–657, 1987.
- Bernabe, Y., Pore geometry and pressure dependence of the transport properties in sandstones, *Geophysics*, 56, 436–446, 1991.
- Berryman, J. G., Effective stress for transport properties of inhomogeneous porous rock, *J. Geophys. Res.*, 97, 17,409–17,424, 1992.
- Berryman, J. G., Effective-stress rules for pore-fluid transport in rocks containing two minerals, *Int. J. Rock Mech. Min. Sci.*, 30, 1165–1168, 1993.
- Berryman, J. G., and S. C. Blair, Use of digital image analysis to estimate fluid permeability of porous materials: Application of two-point correlation functions, *J. Appl. Phys.*, 60, 1930–1938, 1986.
- Berryman, J. G., and S. C. Blair, Kozeny-Carmen relations and image processing methods for estimating Darcy's constant, *J. Appl. Phys.*, 62, 2221–2228, 1987.
- Bigelow, E. L., Global occurrences of abnormal pressures, in *Studies in Abnormal Pressures*, edited by W. H. Fertl, R. E. Chapman, and R. F. Hotz, pp. 1–17, Elsevier Sci., New York, 1994.
- Biot, M. A., General theory of three-dimensional consolidation, *J. Appl. Phys.*, 12, 155–164, 1941.
- Biot, M. A., and D. G. Willis, The elastic coefficients of the theory of consolidation, *J. Appl. Mech.*, 24, 594–601, 1957.
- Bishop, R. S., Calculated compaction states of thick abnormally pressured shales, *AAPG Bull.*, 63, 918–933, 1979.
- Blair, S. C., P. A. Berge, and J. G. Berryman, Using two-point correlation functions to characterize microgeometry and estimate permeabilities of sandstones and porous glass, *J. Geophys. Res.*, 101, 20,359–20,375, 1996.
- Brace, W. F., Permeability of crystalline and argillaceous rocks, *Int. J. Rock Mech. Min. Sci. Geomech. Abstr.*, 17, 241–251, 1980.
- Brace, W. F., J. B. Walsh, and W. T. Frangos, Permeability of granite under high pressure, *J. Geophys. Res.*, 73, 2225–2236, 1968.
- Braddock, W. A., and M. Machette, Experimental deformation of Pierre shale, final report, 96 pp., U.S. Air Force Geophys. Lab., Hanscom Air Force Base, Mass., 1976.
- Bradley, J. S., Abnormal formation pressure, *Am. Assoc. Pet. Geol. Bull.*, 59, 957–973, 1975.
- Bredehoeft, J. D., and B. B. Hanshaw, On the maintenance of anomalous fluid pressures, I, Thick sedimentary sequences, *Geol. Soc. Am. Bull.*, 79, 1097–1106, 1968.
- Bredehoeft, J. D., C. E. Neuzil, and P. C. D. Milly, Regional flow in the Dakota aquifer—A study of the role of confining layers, *U.S. Geol. Surv. Water Supply Pap.*, 2237, 45 pp., 1983.
- Brighenti, G., Effect of confining pressure on gas permeability of tight sandstones, in *Rock at Great Depth*, edited by V. Maury and D. Foumaintraux, pp. 187–194, A. A. Balkema, Brookfield, Vt., 1989.
- Brown, S. R., Fluid flow through rock joints: The effect of surface roughness, *J. Geophys. Res.*, 92, 1337–1347, 1987.
- Brown, S. R., and R. L. Bruhn, Fluid permeability of deformable fracture networks, *J. Geophys. Res.*, 103, 2489–2500, 1998.
- Brown, S. R., and C. H. Scholz, Closure of random elastic surfaces in contact, *J. Geophys. Res.*, 90, 5531–5545, 1985.
- Brown, S. R., H. W. Stockman, and S. J. Reeves, Applicability of the Reynolds equation for modeling fluid flow between rough surfaces, *Geophys. Res. Lett.*, 22, 2537–2540, 1995.
- Bruce, C. H., Pressured shale and related sediment deformation—Mechanism for development of regional contemporaneous faults, *Am. Assoc. Pet. Geol. Bull.*, 57, 878–886, 1973.
- Bruce, C. H., Smectite dehydration—Its relation to structural development and hydrocarbon accumulation in northern Gulf of Mexico Basin, *AAPG Bull.*, 68, 673–683, 1984.
- Bryant, W. R., W. Hottman, and P. Trabant, Permeability of unconsolidated and consolidated marine sediments, Gulf of Mexico, *Mar. Geotechnol.*, 1, 1–14, 1975.
- Burst, J. F., Diagenesis of Gulf Coast clayey sediments and its possible relation to petroleum migration, *Am. Assoc. Pet. Geol. Bull.*, 53, 73–93, 1969.
- Caillet, G., The caprock of the Snorre Field, Norway—A possible leakage by hydraulic fracturing, *Mar. Pet. Geol.*, 10, 42–50, 1993.
- Carlson, R. L., and A. F. Gangi, Effect of cracks on the pressure dependence of P wave velocities in crystalline rocks, *J. Geophys. Res.*, 90, 8675–8684, 1985.
- Chapman, R. E., Clays with abnormal interstitial fluid pressures, *Am. Assoc. Pet. Geol. Bull.*, 56, 790–795, 1972.
- Chapman, R. E., The geology of abnormal pore pressures, in *Studies in Abnormal Pressures*, edited by W. H. Fertl, R. E. Chapman, and R. F. Hotz, pp. 19–49, Elsevier Sci., New York, 1994a.
- Chapman, R. E., Abnormal pore pressures—Essential theory, possible causes, and sliding, in *Studies in Abnormal Pressures*, edited by W. H. Fertl, R. E. Chapman, and R. F. Hotz, pp. 51–91, Elsevier Sci., New York, 1994b.
- Chen, C. T., L. S. Chen, and F. J. Millero, Speed of sound in NaCl, MgCl₂, Na₂SO₄, and MgSO₄ aqueous solutions as functions of concentration, temperature, and pressure, *J. Acoust. Soc. Am.*, 63, 1975–1800, 1978.
- Christensen, N. I., and H. F. Wang, The influence of pore pressure and confining pressure on dynamic elastic properties of Berea sandstone, *Geophysics*, 50, 207–213, 1985.
- David, C., Geometry of flow paths for fluid transport in rocks, *J. Geophys. Res.*, 98, 12,267–12,278, 1993.
- David, C., and M. Darot, Permeability and conductivity of sandstones, in *Rock at Great Depth*, edited by V. Maury and D. Foumaintraux, pp. 203–209, A. A. Balkema, Brookfield, Vt., 1989.
- David, C., Y. Gueguen, and G. Pampoukis, Effective medium theory and network theory applied to the transport properties of rock, *J. Geophys. Res.*, 95, 6993–7005, 1990.
- Deming, D., Factors necessary to define a pressure seal, *AAPG Bull.*, 78, 1005–1009, 1994.
- Dewhurst, D. N., A. C. Aplin, J.-P. Sarda, and Y. Yang, Compaction-driven evolution of porosity and permeability in natural mudstones: An experimental study, *J. Geophys. Res.*, 103, 651–661, 1998.
- Dewhurst, D. N., A. C. Aplin, and J.-P. Sarda, Influence of clay fraction on pore-scale properties and hydraulic conductivity of experimentally compacted mudstones, *J. Geophys. Res.*, 104, 29,261–29,274, 1999.
- Dickey, P. A., C. R. Shriram, and W. R. Paine, Abnormal pressures in deep wells of southwestern Louisiana, *Science*, 160, 609–615, 1968.
- Dickinson, G., Geological aspects of abnormal reservoir pressures in Gulf Coast Louisiana, *Am. Assoc. Pet. Geol. Bull.*, 37, 410–432, 1953.
- Doyen, P. M., Permeability, conductivity, and pore geometry of sandstone, *J. Geophys. Res.*, 93, 7729–7740, 1988.
- Dzevanshir, R. D., L. A. Buryakovskiy, and G. V. Chilingarian, Simple quantitative evaluation of porosity of argillaceous sediments at various depths of burial, *Sediment. Geol.*, 46, 169–175, 1986.
- Eberl, D., and J. Hower, Kinetics of illite formation, *Geol. Soc. Am. Bull.*, 87, 1326–1330, 1976.
- Fatt, I., Compressibility of sandstones at low to moderate pressures, *Am. Assoc. Pet. Geol. Bull.*, 42, 1924–1957, 1958.
- Fatt, I., The Biot-Willis elastic coefficients for a sandstone, *J. Appl. Mech.*, 26, 296–297, 1959.
- Fredrich, J. T., K. H. Greaves, and J. W. Martin, Pore geometry and transport properties of Fontainebleau sandstone, *Int. J. Rock Mech. Min. Sci. Geomech. Abstr.*, 30, 691–697, 1993.
- Gangi, A. F., Hertz theory applied to the porosity-pressure, permeability-pressure and failure strength-porosity variations of porous rocks, *Proc. U.S. Rock Mech. Symp.*, 17th, 2A5-1–2A5-8, 1976.
- Gangi, A. F., Variation of whole and fractured porous rock permeability with confining pressure, *Int. J. Rock Mech. Min. Sci. Geomech. Abstr.*, 15, 249–257, 1978.
- Gangi, A. F., and R. L. Carlson, An asperity-deformation model for effective pressure, *Tectonophysics*, 256, 241–251, 1996.
- Garg, S. K., and A. Nur, Effective stress laws for fluid-saturated porous rocks, *J. Geophys. Res.*, 78, 5911–5921, 1973.
- Green, D. H., and H. F. Wang, Fluid pressure response to undrained compression in saturated sedimentary rock, *Geophysics*, 51, 948–956, 1986.
- Han, D.-H., A. Nur, and D. Morgan, Effects of porosity and clay

- content on wave velocities in sandstones, *Geophysics*, 51, 2093–2107, 1986.
- Handin, J., R. V. Hager, M. Friedman, and J. N. Feather, Experimental deformation of sedimentary rocks under confining pressure—Pore pressure tests, *Am. Assoc. Pet. Geol. Bull.*, 47, 717–755, 1963.
- Harrison, W. J., and L. Summa, Paleohydrology of the Gulf of Mexico Basin, *Am. J. Sci.*, 291, 109–176, 1991.
- Hornby, B. E., The elastic properties of shales, Ph.D. dissertation, Univ. of Cambridge, Cambridge, England, 1994.
- Howard, J. J., Influence of authigenic-clay minerals on permeability, in *Origin, Diagenesis, and Petrophysics of Clay Minerals in Sandstones*, edited by D. W. Houseknecht and E. D. Pittman, *Spec. Publ. SEPM*, 47, 257–264, 1992.
- Hubbert, M. K., and W. W. Rubey, Role of fluid pressure in mechanics of overthrust faulting, I, Mechanics of fluid-filled porous solids and its application to overthrust faulting, *Geol. Soc. Am. Bull.*, 70, 115–166, 1959.
- Hunt, J. M., Generation and migration of petroleum from abnormally pressured fluid compartments, *AAPG Bull.*, 74, 1–12, 1990.
- Ibanez, W. D., and A. K. Kronenberg, Experimental deformation of shale: Mechanical properties and microstructural indicators of mechanisms, *Int. J. Rock Mech. Min. Sci. Geomech. Abstr.*, 30, 723–734, 1993.
- Ives, K. J., Filtration of clay suspensions through sand, *Clay Miner.*, 22, 49–61, 1987.
- Johnston, D. H., Physical properties of shale at temperature and pressure, *Geophysics*, 52, 1391–1401, 1987.
- Johnston, J. E., and N. I. Christensen, Seismic anisotropy of shales, *J. Geophys. Res.*, 100, 5991–6003, 1995.
- Jones, F. O., Jr., A laboratory study of the effects of confining pressure on fracture flow and storage capacity in carbonate rocks, *J. Pet. Technol.*, 27, 21–27, 1975.
- Jones, F. O., Jr., and W. W. Owens, A laboratory study of low-permeability gas sands, *J. Pet. Technol.*, 32, 1631–1640, 1980.
- Karig, D. E., and G. Hou, High-stress consolidation experiments and their geologic implications, *J. Geophys. Res.*, 97, 289–300, 1992.
- Katsube, T. J., B. S. Mudford, and M. E. Best, Petrophysical characteristics of shales from the Scotian Shelf, *Geophysics*, 56, 1681–1689, 1991.
- Kim, J. W., W. R. Bryant, J. S. Watkins, and T. T. Tieh, Mineralogical and fabric changes of shale during burial diagenesis and their effects on petrophysical properties, *Trans. Gulf Coast Assoc. Geol. Soc.*, 48, 139–150, 1998.
- Kim, J. W., W. R. Bryant, J. S. Watkins, and T. T. Tieh, Electron microscopic observations of shale diagenesis, offshore Louisiana, USA, Gulf of Mexico, *Geo Mar. Lett.*, 18, 234–240, 1999.
- Kranz, R. L., A. D. Frankel, T. Engelder, and C. H. Scholz, The permeability of whole and jointed Barre granite, *Int. J. Rock Mech. Min. Sci. Geomech. Abstr.*, 16, 225–234, 1979.
- Kwon, O., and A. K. Kronenberg, Deformation of Wilcox shale: Undrained strengths and effects of strain rate, in *Proceedings of the 1st North American Rock Mechanics Symposium*, edited by P. P. Nelson and S. E. Laubach, pp. 757–765, A. A. Balkema, Brookfield, Vt., 1994.
- Lee, J. H., J. H. Ahn, and D. Peacor, Textures in layered silicates: Progressive changes through diagenesis and low temperature metamorphism, *J. Sediment Petrol.*, 55, 532–540, 1985.
- Lide, D. R., *CRC Handbook of Chemistry and Physics*, 78th ed., pp. 1–62, CRC Press, Boca Raton, Fla., 1997.
- Lin, W., Measuring the permeability of Eleana argillite from area 17, Nevada test site, using the transient method, *Rep. UCRL-52604*, 11 pp., Lawrence Livermore Natl. Lab., Livermore, Calif., 1978.
- Magara, K., Permeability considerations in generation of abnormal pressures, *Soc. Pet. Eng. J.*, 11, 236–242, 1971.
- Magara, K., *Compaction and Fluid Migration: Practical Petroleum Geology*, 319 pp., Elsevier Sci., New York, 1978.
- Meyer, C. A., R. B. McClintock, G. J. Silvestri, and R. C. Spence, Jr., *ASME Steam Table, Thermodynamic and Transport Properties of Steam*, 330 pp., Am. Soc. of Mech. Eng., New York, 1979.
- Millero, F. J., G. K. Ward, and P. V. Chetirkin, Relative sound velocities of sea salts at 25°C, *J. Acoust. Soc. Am.*, 61, 1492–1498, 1977.
- Morrow, C. A., L. Q. Shi, and J. D. Byerlee, Permeability of fault gouge under confining pressure and shear stress, *J. Geophys. Res.*, 89, 3193–3200, 1984.
- Morrow, C. A., B.-C. Zhang, and J. D. Byerlee, Effective pressure law for permeability of Westerly granite under cyclic loading, *J. Geophys. Res.*, 91, 3870–3876, 1986.
- Nagtegaal, P., Relationship of facies and reservoir quality in Rotliegendes desert sandstones, southern North Sea region, *J. Pet. Geol.*, 2, 145–158, 1979.
- Neglia, S., Migration of fluids in sedimentary basins, *AAPG Bull.*, 63, 573–597, 1979.
- Nelson, R. A., An experimental study of fracture permeability in porous rock, *Proc. U.S. Symp. Rock Mech.*, 17th, 2A6-1–2A6-8, 1976.
- Neuzil, C. E., How permeable are clays and shales?, *Water Resour. Res.*, 30, 145–150, 1994.
- Nur, A., and J. D. Byerlee, An exact effective stress law for elastic deformation of rock with fluids, *J. Geophys. Res.*, 76, 6414–6419, 1971.
- Olgaard, D. L., R. Nuesch, and J. Urai, Consolidation of water saturated shales at great depth under drained conditions, in *Rock Mechanics: Proceedings of the 8th International Congress on Rock Mechanics*, edited by T. Fujii, 273–277, A. A. Balkema, Brookfield, Vt., 1995.
- Olsen, H. W., Liquid movement through kaolinite under hydraulic, electric, and osmotic gradients, *Am. Assoc. Pet. Geol. Bull.*, 56, 2022–2028, 1972.
- Pallatt, N., J. Wilson, and B. McHardy, The relationship between permeability and the morphology of diagenetic illite in reservoir rocks, *J. Pet. Technol.*, 36, 2225–2227, 1984.
- Paterson, M. S., *Experimental Rock Deformation—The Brittle Field*, 254 pp., Springer-Verlag, New York, 1978.
- Paterson, M. S., The equivalent channel model for permeability and resistivity in fluid-saturated rock—A reappraisal, *Mech. Mater.*, 2, 345–352, 1983.
- Plumley, W. J., Abnormally high fluid pressure—Survey of some basic principles, *AAPG Bull.*, 64, 414–430, 1980.
- Rice, J. R., and M. P. Cleary, Some basic stress diffusion solutions for fluid-saturated elastic porous media with compressible constituents, *Rev. Geophys.*, 14, 227–241, 1976.
- Robin, P.-Y. F., Note on effective pressure, *J. Geophys. Res.*, 78, 2434–2437, 1973.
- Schlomer, S., and B. M. Krooss, Experimental characterization of the hydrocarbon sealing efficiency of cap rocks, *Mar. Pet. Geol.*, 14, 565–580, 1997.
- Schmidt, G. W., Interstitial water composition and geochemistry of deep Gulf Coast shales and sandstones, *Am. Assoc. Pet. Geol. Bull.*, 57, 321–337, 1973.
- Schofield, A., and P. Wroth, *Critical State Soil Mechanics*, 310 pp., McGraw-Hill, New York, 1968.
- Scott, C. R., *An Introduction to Soil Mechanics and Foundations*, 406 pp., Elsevier Sci., New York, 1980.
- Seeburger, D. A., and A. Nur, A pore space model for rock permeability and bulk modulus, *J. Geophys. Res.*, 89, 527–536, 1984.
- Silva, A. J., J. R. Hetherman, and D. I. Calnan, Low-gradient permeability testing of fine-grained marine sediments, in *Permeability and Groundwater Contaminant Transport*, edited by T. F. Zimmie and C. O. Riggs, *ASTM Spec. Tech. Publ.*, 746, 121–136, 1981.
- Skempton, A. W., Effective stress in soils, concrete and rocks, in *Conference on Pore Pressure and Suction in Soils*, pp. 4–16, Butterworths, London, 1961.
- Stalder, P. J., Influence of crystallographic habit and aggregate structure of authigenic clay minerals on sandstone permeability, *Geol. Mijnbouw*, 52, 217–220, 1973.
- Sutherland, H. J., and S. P. Cave, Argon gas permeability of New Mexico rock salt under hydrostatic compression, *Int. J. Rock Mech. Min. Sci.*, 17, 281–288, 1980.
- Swan, G., J. Cook, S. Bruce, and R. Meehan, Strain rate effects in Kimmeridge Bay shale, *Int. J. Rock Mech. Min. Sci. Geomech. Abstr.*, 26, 135–149, 1989.
- Tavenas, F., P. Jean, P. Leblond, and S. Leroueil, The permeability of natural soft clays, II, Permeability characteristics, *Can. Geotech. J.*, 20, 645–660, 1983.
- Terzaghi, K., Die berechnung der durchlässigkeitsziffer des tones aus dem verlauf der hydrodynamischen spannungserscheinungen, *Sitzungsber. Akad. Wiss. Wien Math Naturwiss. Kl. Abt. IIa*, 132, 105–124, 1923.
- Terzaghi, K., Principles of soil mechanics, *Eng. News Rec.*, 95, 987–996, 1925.
- Terzaghi, K., The shearing resistance of saturated soils and the angle between the planes of shear, in *Proceedings of the 1st International*

- Conference on Soil Mechanics and Foundation Engineering*, pp. 54–56, Harvard Univ. Press, Cambridge, Mass., 1936.
- Thompson, A. H., A. J. Katz, and C. E. Krohn, The microgeometry and transport properties of sedimentary rock, *Adv. Phys.*, *36*, 625–694, 1987.
- Todd, T., and G. Simmons, Effect of pore pressure on the velocity of compressional waves in low-porosity rocks, *J. Geophys. Res.*, *77*, 3731–3743, 1972.
- Trimmer, D. A., Design criteria for laboratory measurements of low permeability rocks, *Geophys. Res. Lett.*, *8*, 973–975, 1981.
- Vasseur, G., I. Djeran-Maigre, D. Grunberger, G. Rousset, D. Tessier, and B. Velde, Evolution of structural and physical parameters of clays during experimental compaction, *Mar. Pet. Geol.*, *12*, 941–954, 1995.
- Vernik, L., and X. Liu, Velocity anisotropy in shales: A petrophysical study, *Geophysics*, *62*, 521–532, 1997.
- Vernik, L., and A. Nur, Ultrasonic velocity and anisotropy of hydrocarbon source rocks, *Geophysics*, *57*, 727–735, 1992.
- Walls, J., and A. Nur, Pore pressure and confining pressure dependence of permeability in sandstone, paper presented at 7th Formation Evaluation Symposium, Can. Well Logging Soc., Calgary, Alberta, 1979.
- Walsh, J. B., Effect of pore pressure and confining pressure on fracture permeability, *Int. J. Rock Mech. Min. Sci.*, *18*, 429–435, 1981.
- Walsh, J. B., and W. F. Brace, The effect of pressure on porosity and the transport properties of rock, *J. Geophys. Res.*, *89*, 9425–9431, 1984.
- Walsh, J. B., and M. A. Grosebaugh, A new model for analyzing the effect of fractures on compressibility, *J. Geophys. Res.*, *84*, 3532–3536, 1979.
- Witherspoon, P. A., J. S. Y. Wang, K. Iwai, and J. E. Gale, Validity of cubic law for fluid flow in a deformable rock fracture, *Water Resour. Res.*, *16*, 1016–1024, 1980.
- Wolf, A. V., M. G. Brown, and P. G. Prentiss, Concentrative properties of aqueous solutions: Conversion tables, in *CRC Handbook of Chemistry and Physics*, 60th ed., edited by R. C. Weast, pp. D227–D276, CRC Press, Boca Raton, Fla., 1979.
- Wong, T.-f., J. T. Fredrich, and G. D. Gwanmesia, Crack aperture statistics and pore space fractal geometry of Westerly granite and Rutland quartzite: Implications for an elastic contact model of rock compressibility, *J. Geophys. Res.*, *94*, 10,267–10,278, 1989.
- Wood, D. M., *Soil Behaviour and Critical State Soil Mechanics*, 462 pp., Cambridge Univ. Press, New York, 1990.
- York, D., Least squares fitting of a straight line, *Can. J. Phys.*, *44*, 1079–1086, 1966.
- Young, A., P. F. Low, and A. S. McLatchie, Permeability studies of argillaceous rocks, *J. Geophys. Res.*, *69*, 4237–4245, 1964.
- Zhu, W., C. David, and T.-F. Wong, Network modeling of permeability evolution during cementation and hot isostatic pressing, *J. Geophys. Res.*, *100*, 15,451–15,464, 1995.
- Zhu, W., B. Evans, and Y. Bernabe, Densification and permeability reduction in hot-pressed calcite: A kinetic model, *J. Geophys. Res.*, *104*, 25,501–25,511, 1999.
- Zoback, M. D., High pressure deformation and fluid flow in sandstone, granite, and granular materials, Ph.D. thesis, Stanford Univ., Stanford, Calif., 1975.
- Zoback, M. D., and J. D. Byerlee, Permeability and effective stress, *Am. Assoc. Pet. Geol. Bull.*, *59*, 154–158, 1975.
- Zoback, M. D., and J. D. Byerlee, Effect of high-pressure deformation on permeability of Ottawa sand, *Am. Assoc. Pet. Geol. Bull.*, *60*, 1531–1542, 1976.
- A. F. Gangi, B. Johnson, A. K. Kronenberg, and O. Kwon, Center for Tectonophysics, Department of Geology and Geophysics, Texas A&M University, College Station, TX 77843, USA. (gangi@geo.tamu.edu; johnson@geo.tamu.edu; a-kronenberg@tamu.edu; kwon@geo.tamu.edu)

(Received August 16, 2000; revised May 11, 2001; accepted May 14, 2001.)

